

Multiscale modeling of submonolayer growth for Fe/Mo(110)

M Mašín¹, M Kotrla¹, B Yang², M Asta³, M O Jahma⁴
and T Ala-Nissila^{4,5}

¹Institute of Physics, Academy of Science of the Czech Republic, Na Slovance 2, Prague, 18221, Czech Republic

²Department of Chemical Engineering and Materials Science, University of California, Davis, CA 95616, USA.

³Department of Materials Science and Engineering University of California Berkeley, Berkeley, California 94720, USA.

⁴COMP CoE at the Department of Applied Physics, Aalto University School of Science, P.O. Box 11000, FI-00076 Aalto, Espoo, Finland

⁵Department of Physics, Brown University, Providence RI 02912-1843

E-mail: kotrla@fzu.cz

Abstract. We use a multiscale approach to study a lattice-gas model of submonolayer growth of Fe/Mo(110) by Molecular Beam Epitaxy. To begin with, we construct a two-dimensional lattice-gas model of the Fe/Mo(110) system based on first-principles calculations of the monomer diffusion barrier and adatom-adatom interactions. The model is investigated by equilibrium Monte Carlo (MC) simulations to compute the diffusion coefficients of Fe islands of different sizes. These quantities are then used as input to the coarse-grained Kinetic Rate Equation (KRE) approach, which provides time evolution of the island size distributions for a system undergoing diffusion driven aggregation within the 2D submonolayer regime. We calculate these distributions at temperatures $T = 500$ K and 1000 K using the KRE method. We also employ direct kinetic MC simulations of our model to study island growth at $T = 500$ K, and find good agreement with the KRE results, which validates our multi-scale approach.

PACS numbers: 81.15.Aa, 68.43.Jk, 68.55.A-, 05.10.-a

1. Introduction

Basic concepts of growth of thin films were already developed in the last century, in particular in the context of the classical nucleation theory (for a review see e.g. [1, 2]). Most recently, increased effort has been devoted to understanding surface growth at the microscopic level both experimentally and theoretically (for review see e.g. [3, 4] and references therein). Due to the inherently complicated nature of surface growth processes numerical simulation methods at atomic scales, such as kinetic Monte Carlo (KMC) and Molecular Dynamics (MD) methods, have played an important role in modeling surface growth. However, realistic modeling of surface growth in metallic systems under Molecular Beam Epitaxy (MBE) conditions is a challenging problem, which in addition to atomic scale simulation methods benefits greatly from development of efficient multi-scale models. One of the main challenges in trying to model MBE growth processes at atomic scales stems from the large difference between the deposition and diffusion time scales under typical MBE conditions. In addition, classical activation barriers controlling atomic diffusion mechanisms on growing surfaces may span a wide range of values, from meV to eV scales. This makes it impractical to apply classical MD simulations without using flux values that are orders of magnitude larger than those in MBE. This naturally raises serious doubts concerning the validity of such simulations to faithfully describe MBE.

To this end, atomistic calculations (using either *ab initio* or classical semi-empirical potentials) have been frequently employed to construct solid-on-solid (SOS) type of interaction Hamiltonians, which can then be used in kinetic Monte Carlo simulations. Such KMC simulations are applicable to scales from hundreds to a few thousands of atomic distances. Although significant progress has been recently made in speeding up KMC simulations [5, 6] they remain computationally demanding in most realistic cases. Thus, appropriately coarse-grained methods are beneficial. One such promising approach is based on describing the kinetics of growth with the classical kinetic rate equation (KRE) approach [7, 8, 9, 10]. It has been shown by extensive studies that the KRE approach can accurately describe 2D growth processes in cases where spatial correlations do not play an important role. The main advantage of the KRE approach over atomistic simulation methods is that the numerical effort required is relatively insensitive to the ratio between the deposition flux and adatom diffusion scales, and thus realistic growth parameter values can be easily studied (including fluxes much less than 1 ML/s). The conceptual simplicity of the KRE theory also allows easy adjustment of the various growth processes and their rates. Most recently, an improved self-consistent KRE approach to irreversible island growth has been developed by Hubartt *et al.* [11], which accurately reproduces results obtained from KMC simulations.

As far as specific systems are concerned there exist a number of experimental studies with atomistic resolution for different metals on bcc(110) surfaces, which are of great current interest because many of the important magnetic metals have bcc crystal structure. For example, Fe on Fe(110) [12, 13], Fe on W(110) or Mo(110) [14], and

Cu on W(110) [15] have been studied. Modeling and understanding of growth on this anisotropic surface is still very limited. In the case of homoepitaxy, there are atomistic KMC simulations of Fe/Fe(110) homoepitaxy [12, 13], and simulations of a niobium film by molecular dynamics [16]. On a larger length scale there is a qualitative phase-field simulation of stripe arrays observed in multilayer growth on a bcc(110) surface [17]. In the case of heteroepitaxy, modeling becomes even more complex because in addition to anisotropy one should take into account also strain (lattice mismatch) effects. As regards atomistic modeling of bcc(110) surfaces there are, to our knowledge, only two published KMC simulations: investigation of low temperature MBE growth of Cu on W(110) [18] and study of island morphology in the Fe/Mo(110) system [19]. These simulations use lattice gas models with effective parameters for the heteroepitaxial system. Therefore, the effect of strain is included only indirectly. Another deficit in these studies is that adatom diffusion, which plays a predominant role in MBE growth, is not described in terms of realistic energy parameters. The situation for heteroepitaxy on bcc(110) surfaces is in this sense unsatisfactory so far. Contrary to many calculations of diffusion barriers on fcc surfaces, e.g. in the case of well studied Pt/P(111) system [20], there are only a few results for the quantitative values of diffusion barriers on bcc(110) surfaces [21].

In this work, we present a comprehensive multiscale study of heteroepitaxial growth on a bcc(110) surface in the submonolayer regime. Our aim is to present a multiscale modeling strategy using data obtained from microscopic *ab initio* electronic structure calculations as a basis to construct models, which allow numerical studies of MBE growth. As a specific system, we have chosen Fe heteroepitaxy on Mo(110) due to its interesting applications to magnetic nanoislands [22, 23]. The lattice mismatch between Fe and Mo is relatively large (-9%) and thus we restrict the modeling here to early stages of growth, *i.e.* to the submonolayer regime of 2D island growth, which is dominated by deposition and surface diffusion of Fe adatoms. It is known that strain influences surface diffusion [24] in such a way that tensile strain in general leads to a decrease of diffusion barriers [25, 26]. In our case this effect is included in the first-principles energy barriers obtained for Fe diffusion. In this work no other strain effects are included. Using the *ab initio* data we then construct a lattice-gas Hamiltonian with correct energetics, and use this Hamiltonian in KMC simulations. Further, we employ equilibrium MC simulations to calculate diffusion coefficients of islands of various sizes. With these data we construct a KRE aggregation model, which can then be used to study island size distribution development on different scales and in different growth regimes. We compare results obtained from KMC and KRE approaches and find good agreement between the two methods.

2. Model and quantities calculated

2.1. Submonolayer model for Fe/Mo(110)

We begin by constructing a growth model of the Fe/Mo(110) surface, which will be used to study diffusion and growth of Fe adatoms on an ideal Mo(110) surface. It is based on the well-established solid-on-solid (SOS) model of epitaxial growth [27] that has been shown to be capable of reproducing many aspects of epitaxial growth, including scaling of island densities [28]. In the SOS approach neither vacancies nor overhangs are permitted, and the substrate is assumed to have the bcc(110) structure with no steps. In the present work we apply this model in the range of submonolayer coverage, which means that it corresponds to a 2D lattice-gas model, where diffusion is restricted to the 2D surface and particle deposition occurs on empty lattice sites only. We consider lateral interactions up to sixth-nearest neighbors as shown schematically in figure 1.

To construct the atomistic model, we first need to determine the relevant Fe-Mo and Fe-Fe adatom interactions on the Mo(110) surface. It is experimentally known [29] that a monolayer of Fe deposited on Mo(110) forms a commensurate layer and thus we take the adsorption sites of the Fe adatoms to be on top of the second atomic layer of the Mo(110) surface, as shown in figure 1. The interaction with the substrate is characterized by a hopping barrier for diffusion of a free adatom, described by an activation energy E_d . We consider Fe-Fe adatom interactions up to sixth-nearest neighbors described by six binding energies E_{Bk} , $k = 1, \dots, 6$. To compute the activation energies and binding energies we performed first-principles calculations within the framework of density-functional theory, employing ultrasoft pseudopotentials [30], as implemented in the Vienna ab initio simulation package (VASP) [31, 32]. Calculations were performed employing the 1991 generalized gradient approximation of Perdew and Wang [33] and the pseudopotentials labeled "Mo" and "Fe" in the VASP library.

The activation energies and binding energies reported here were obtained from spin-polarized calculations employing slab supercells containing seven Mo layers with lateral periodic lengths corresponding to 4×4 primitive unit cells on the Mo(110) surface. In the calculations Fe adatoms were arranged in appropriate configurations on top and bottom surfaces. A plane-wave cutoff of 300 eV and k -point mesh of $4 \times 4 \times 1$ were employed in all calculations. A series of calculations was undertaken to check the convergence of the results with respect to plane-wave cutoff, slab and vacuum thickness, and the lateral periodic dimensions of the supercell. Based on these calculations the activation energy is estimated to be converged numerically to within a few times 0.01 eV. Using the above procedure, we obtained the following values of the model parameters: $E_d = 0.41$ eV, $E_{B1} = 329$ meV, $E_{B2} = 72$ meV, $E_{B3} = 79$ meV, $E_{B4} = -10$ meV, $E_{B5} = -4.1$ meV, and $E_{B6} = 7.5$ meV. In the present 2D case it can be immediately concluded that the last three values are probably small enough to be omitted in the simulations. We have verified this by testing their influence, which will be discussed in section 2.2.

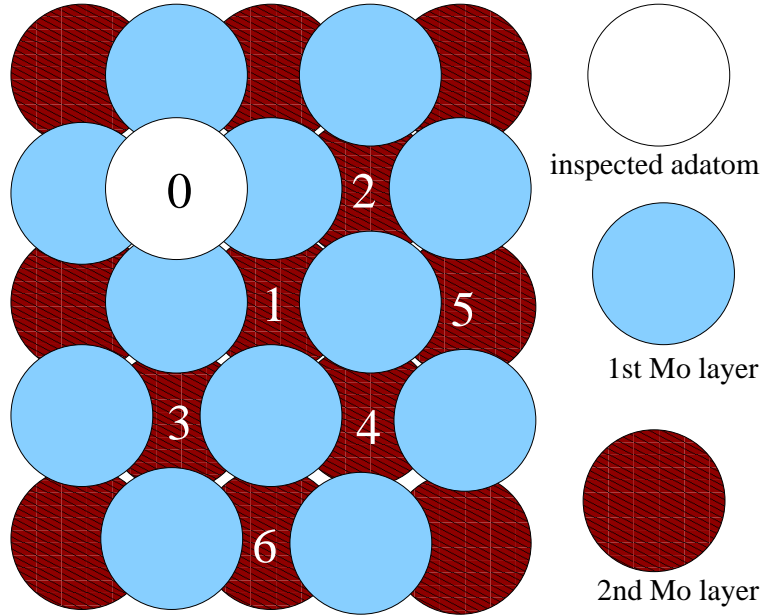


Figure 1. (Colour online) A schematic of an ideal Mo(110) surface, with one Fe adatom occupying site 0, which is an on-top site for the *second* layer Mo atoms. A second Fe adatom that forms a Fe-Fe dimer can then occupy different neighboring positions, such as 1 (nearest neighbor), 2 (second nearest neighbor), and so on up to 6th nearest neighbors in the present case.

2.2. Calculation of adatom island diffusion coefficients

As the first step in the construction of a coarse-grained growth model based on the KRE approach we need to determine the tracer diffusion coefficients $D_s(T)$ of islands of size s . In this work, they are determined using equilibrium Monte Carlo simulations. Based on the previous section, the corresponding 2D lattice-gas Hamiltonian reads

$$H = - \sum_{k=1}^6 \sum_{|i-j|=k, i>j} E_{Bk} m_i m_j, \quad (1)$$

which includes pair interactions E_{Bk} only up to sixth neighbors. Here, $m_i = 0, 1$ is the occupation number of a lattice site i . We note that equation (1) corresponds to simple bond counting between each pair of Fe adatoms.

Diffusion is modeled by thermally activated hops of Fe adatoms to a vacant nearest neighbor position. In this section, our model is studied by standard Monte Carlo simulations with Metropolis dynamics using the transition dynamics algorithm (TDA), which is a good choice for calculation of diffusion coefficients and is described in detail in Refs. [34, 35]. The jump probability in TDA depends on the energies in initial and final sites and the saddle point energy. The energy of the saddle point is calculated as an arithmetic mean of the energies of the initial and final sites, including the diffusion barrier for a free adatom, *i.e.*

$$E_S = \frac{1}{2} (E_i + E_f) + E_d. \quad (2)$$

The TDA in our simulations evaluates particle jumps in two successive steps. In the first step, we evaluate the jump probability from the initial site to the saddle point. This step is accepted with the probability $\nu \exp(-\Delta E/kT)$, where $\Delta E = E_S - E_i$, except for the case where the energy of the initial site is higher than the energy of the saddle point, in which case the jump is always accepted (it could occur e.g. in the case of strong adatom-adatom repulsion). The process is repeated for the next step – a move from the saddle point to the final position. This step is accepted with the probability $\nu \exp(-\Delta E/kT)$, where $\Delta E = E_f - E_S$ except for the case when the energy of the saddle point is higher than the energy of the final point. This scheme is more realistic than adding the isolated adatom barrier to half of the difference between the final and initial site energies.

The tracer diffusion coefficient $D_s(T)$ is computed from the mean square displacement of a virtual particle representing the center-of-mass of the whole island:

$$D_s = \lim_{t \rightarrow \infty} \frac{1}{2t} \left\langle \left| \vec{R}_s(t) - \vec{R}_s(0) \right|^2 \right\rangle, \quad (3)$$

where $\vec{R}_s(t) = (1/s) \sum_{j=1}^s [\vec{r}_j(t) - \vec{r}_j(0)]$ represents the position vector of the center-of-mass of the individual island, s is number of particles in the island, and $\vec{r}_j(t)$ is the position of the particle j in the island at the time t . As usual, we have computed $D_s(T)$ by using the memory expansion method [36, 37]. To determine $D_s(T)$ for a given island of size s we prepare an initial configuration composed of s particles comprising one island. Detachment of particles from the island is explicitly forbidden.

We have calculated $D_s(T)$ at two temperatures: $T = 500$ K and $T = 1000$ K. Results of our simulations are shown in figure 2 with data averaged over 20 runs. We note that all the values of D_s are normalized by the prefactor $D_0 = (1/4)\nu_{osc}a^2$, where $a = 3.15$ Å is the lattice constant of Mo and ν_{osc} is the vibrational frequency. There are some clusters with metastable configurations, which cause large error bars for some points in figure 2 at the lower temperature. The diffusion coefficients of islands depend on size non-trivially and can even oscillate as a function of size s [38, 39, 40, 41]. These oscillations can be in part understood by surface geometry: certain close-packed island configurations can be more stable than others [42, 43, 44, 45]. In our calculations, the oscillations as a function of size s are clearly seen at the lower temperature. As temperature increases, the oscillations are dampened, and at our highest temperature the diffusion coefficient is rather well described by $D(s) \sim s^{-3/2}$, which is expected if island diffusion is limited by atomic motion along the perimeter of an island [46, 47]. For Fe/Mo(110), there is a strong dependence of D_s on temperature here because the (bare) single adatom diffusion barrier is about 0.4 eV.

To check the robustness of the diffusion coefficient against the range of Fe-Fe interactions, we performed calculations for three different cases: (i) with nearest neighbor interactions only, (ii) interactions up to third nearest neighbors and (iii) full set of interactions up to sixth nearest neighbors. Figure 2 clearly demonstrates that in the present model the main features of the size dependence of the diffusion coefficient shows the same oscillations for all three different cases studied here. On a quantitative

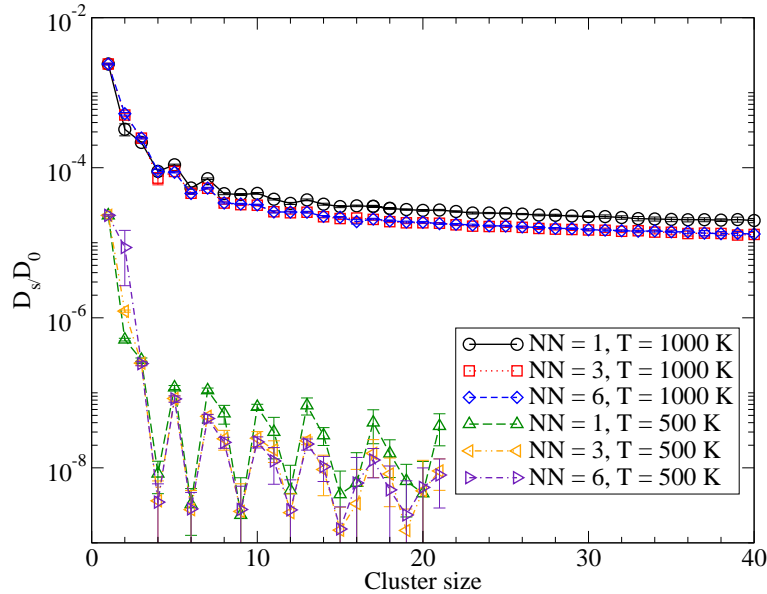


Figure 2. (Colour online) Dependence of normalized diffusion coefficients on island size s for the two temperatures considered here, with three different ranges of interactions, as specified by the label NN (see text for details).

level we can conclude that it is sufficient to include interactions only up to third nearest neighbors when considering KMC simulations of the growth model. This significantly speeds up and simplifies the simulations.

2.3. Island size distribution

The fundamental quantity in 2D island growth is the size distribution function, which characterizes the number density n_s of islands of size s at any given time during growth. For simplified kinetic growth models this function often shows scaling behaviour, which gives valuable information about the growth process [48, 49, 50]. In general, however, there is no theoretical guarantee for the existence such simple scaling solutions. This is true in particular when realistic size-dependent diffusion coefficients are used [51]. However, there can still exist stationary phases of growth, where the effective scaling laws hold in a limited region of parameter space [52].

To this end, in the present work we consider scaled distribution functions, which can be obtained by defining a probability density that a randomly selected atom is contained in an island of size s , viz. $p_s(\theta) = sn_s(\theta)/\theta$, where θ is the surface coverage and n_s is the island number density of islands of size s , *i.e.* the number of islands of size s divided by the number of occupation sites. The average island size is defined as $\bar{s} = M_2/M_1$, where the k^{th} moment of the distribution is given by $M_k = \sum_1^\infty s^k n_s(\theta)$. The scaling function is defined as $g(x) = \bar{s} p_s(\theta)$, where $x = s/\bar{s}$ [52]. In the scaling regime this function becomes independent of coverage for a given set of relevant growth parameters.

3. Numerical studies of island growth

3.1. Atomistic modeling of MBE growth by KMC

The most direct way to study MBE growth of the Fe/Mo(110) system is to employ KMC simulations using the lattice-gas approach. Diffusion is modeled by thermally activated hops of adatoms to unoccupied nearest neighbor positions with a configuration dependent rate. The probability P_i of a jump of an adatom from a site i is exponentially proportional to the product of an activation energy $E_{A(i)}$ and the inverse temperature $1/T$ ‡

$$P_i = \nu_d \exp\left(-\frac{E_{A(i)}}{k_B T}\right), \quad (4)$$

where the prefactor $\nu_d = \nu_s \nu_{osc} = 1.6 \times 10^{13} \text{ s}^{-1}$, and $\nu_s = 4$ is the number of equivalent saddle points and $\nu_{osc} = 4 \times 10^{12}$ is the oscillation frequency. The activation energy $E_{A(i)}$ for the chosen adatom is given by sum of the activation energy for a free particle E_d and the added interactions from neighboring occupied sites. Here, we use the standard bound-counting scheme according to the lattice-gas description. As justified in section II B, we include Fe-Fe interactions up to the third nearest neighbors only. Hence,

$$E_A(i) = E_d + l_1 E_{B1} + l_2 E_{B2} + l_3 E_{B3}, \quad (5)$$

where E_{B1} , E_{B2} , and E_{B3} are interaction energies of the adatom with its lateral first, second and third nearest neighbors, correspondingly, obtained by first-principles calculations in section 2.1. The integer coefficients l_1 , l_2 , and l_3 count the number of occupied first, second, and third nearest neighbors of the site i , correspondingly, which means that $l_1 \in [0, 4]$, $l_2 \in [0, 2]$, and $l_3 \in [0, 2]$.

In our KMC simulations the growth is reversible and it includes process of detachment of an adatom from an island, and breaking of an island. Our KMC simulations are thus consistent with the classical nucleation theory. We note that in our KMC approach islands diffuse by single adatom moves only; no collective adatom events have been implemented here. To maximize the efficiency of the KMC method we utilized the Bortz-Kalos-Lebowitz (BKL) algorithm with the implementation by Maksym [53]. Results reported in the next Section represent simulations on a lattice of the size ranging from 500×500 to 1000×1000 lattice sites, the number of runs varied from 20 up to 1000.

3.2. Kinetic rate equation model of growth

Despite the application of the BKL algorithm to speed up KMC simulations, the microscopic approach is not feasible for large-scale studies of island growth in the micrometer scale. This is mainly due to the fact that in real MBE growth under typical

‡ We note that instead of the TDA algorithm, which we employed for the calculation of the equilibrium island diffusion coefficients, we have here chosen the commonly used simple exponential function to enhance the numerical efficiency of the KMC growth simulations.

conditions the (dimensionless) ratio $\kappa = \Phi a/D_1 \ll 1$. Here Φ is the incoming adatom flux, a is the lattice constant (microscopic length) and D_1 is the single-particle diffusion coefficient. In real units, typical fluxes under MBE conditions are a few monolayers per second, while diffusion coefficients on metal surfaces typically have activation barriers less than 1 eV (here $E_d = 0.4$ eV), leading to $\kappa \ll 1$. Simulating such conditions with KMC is challenging, although most recent work shows that fluxes as small as 10^{-3} are feasible [54].

To facilitate large-scale studies of MBE growth with small values of κ , we employ the coarse-grained kinetic rate equation (KRE) method [8, 9]. The rate equation giving the time evolution of island size distribution n_s for a system undergoing diffusion driven aggregation and with incoming flux Φ of adatoms per monolayer is given by

$$\frac{dn_s(t)}{dt} = \sum_{i+j=s} K(i, j)n_i n_j - \sum_{i=1}^{s-1} K(i, s)n_i n_s + \Phi \delta_{1s}. \quad (6)$$

The function $K(i, j)$ is called aggregation kernel and is given by the usual ansatz

$$K(i, j) = D_i + D_j, \quad (7)$$

where D_i is diffusion coefficient of an adatom island of size i on the surface. In the present model, we neglect adatom detachment from the islands, and explicit island capture rates [11]. In a previous study of submonolayer growth in the Cu/Cu(100) and Cu/Cu(111) systems [51], the island diffusion coefficients were calculated using KMC simulations and then used to calculate the corresponding island size distributions using the KRE approach in the case of hyperthermal deposition. Similar strategy is adapted here for normal MBE growth; however, unlike in reference [51] our energy parameters and thus the diffusion coefficients in figure 2 are based on *ab initio* data.

The coupled set of ordinary differential equations constituting the KRE model give the time evolution of the island size distribution on the surface. It may be solved directly by numerical integration, but given appropriate reaction rates this set of differential equations is usually stiff, thus making the direct approach demanding. In addition, obtaining complete analytic solution is possible only in a limited number of cases with suitable rate coefficients without making strong assumptions about the form of the scaling function. Therefore, we solve these equations using the particle coalescence (PCM) method [55, 56, 52]. In PCM a point-island approximation is used, which is valid at low coverage or large island separations. Aggregation events occur with probabilities specified by the corresponding reaction kernels, and the deposition with the rate proportional to the given adatom flux. An event is then randomly chosen with a probability weighted by the corresponding rate. Since KREs describe the system in the mean-field limit, there is no information on spatial correlations in the system. The main advantage of the KRE approach over KMC simulations, however, is that a wide range of values of κ can be studied, in particular the limit where $\kappa \ll 1$, because all atomistic events in island dynamics are embedded into the effective rates.

In a previous study [9] the island size distributions were found to be of scaling form and the mean island size had a power-law form. Even if the rates were not a

homogeneous functions of the island size, well-defined effective scaling exponents for the mean island size and the size distribution function could be determined. In the present case, we expect that scaling is invalidated due to realistic diffusion coefficients which have a naturally inhomogeneous form, as is evident in figure 2. There is no guarantee of either the existence of usual scaling type of solutions or uniquely defined scaling exponents for the mean island size and island densities. Thus, we have not tried to extract any scaling exponents in the present work.

4. Results and discussion

In this subsection, we consider the scaled distribution function $g(x)$, where $x = \bar{s}/s$. To start with, we have tested the robustness of the growth model by using direct KMC simulations, as described in the previous section. The BKL algorithm allows us to obtain reasonable statistics at the temperature $T = 500$ K if the flux is not too small. We have first considered the case of a high flux of $\Phi = 100$ ML/s (which corresponds to $\Phi/D_1 = 4.3 \times 10^8$ ML/cm²) and checked how the distribution varies with coverage. Here data has been averaged over 20 runs. The results are shown in figure 3. As expected, for a fixed coverage the function has a characteristic form, with a strongly asymmetric peak around $x = 1$. The long tail extending to small island sizes reflects the high mobility of adatoms and small islands. Interestingly enough we find that in all three cases (coverages 0.05, 0.15, and 0.25 ML) the scaled function is almost identical except for the part where $x \ll 1$. The observed decrease of $g(x)$ in the region of small x with increasing coverage is an expected consequence of increased aggregation to large islands. Based on the robustness of the scaled distribution we will only discuss results for the saturation coverage of $\theta = 0.15$ in what follows. We note that at $T = 500$ K the Fe islands have a faceted, rhombic shape, as demonstrated in a recent study using the present lattice-gas model [19].

At the next stage we studied the robustness of $g(x)$ against changing the adatom flux at $T = 500$ K. We found that for the Fe/Mo system it was very hard to acquire any meaningful KMC data for a flux value below $\Phi = 1$ ML/s. Nevertheless, for $\Phi = 1$ ML/s we were able to obtain valid data after extensive averaging. The results are shown in figure 4. The data for $\Phi = 1$ ML/s represent an average over 1000 runs. For comparison, we also calculated the island distribution $\Phi = 10$ ML/s (averaged over 100 runs) and $\Phi = 100$ ML/s (averaged over 20 runs). Despite the poor statistics it can be seen that the scaled distribution is relatively insensitive to the flux, except for $x \ll 1$ where again there is some deviation between the different fluxes. The reason behind this is that even for relatively large fluxes, the fundamental processes involved in island growth are the same and the character of the *scaled* island size distribution relatively insensitive to the flux. However, the important conclusion here is that for the present model the scaled distributions allow us to vary the flux by two orders of magnitude from $\Phi = 1$ ML/s up to 100 ML/s without any significant change in the results.

At the next stage we employed the KRE approach to study island growth. Using

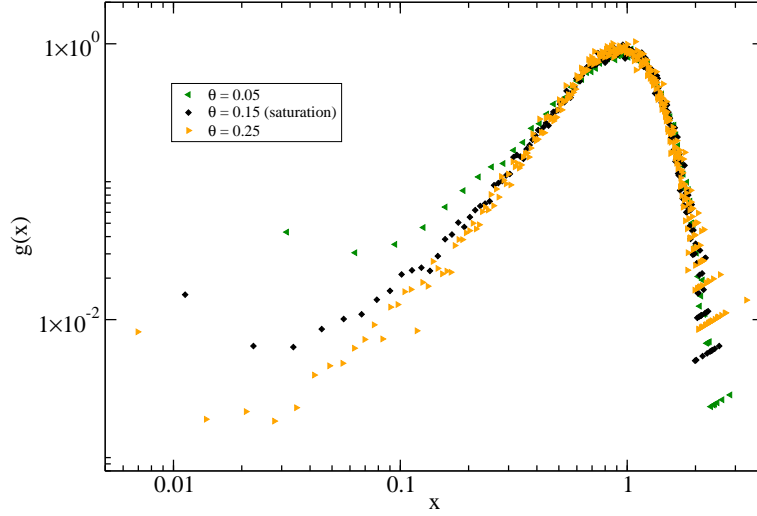


Figure 3. (Colour online) Time development of scaled island size distribution in three different coverage (deposition times), namely $\theta = 0.05$, $\theta = 0.15$ (saturation coverage), and $\theta = 0.25$ for $\Phi = 100$ ML/s and $T = 500$ K using the KMC approach.

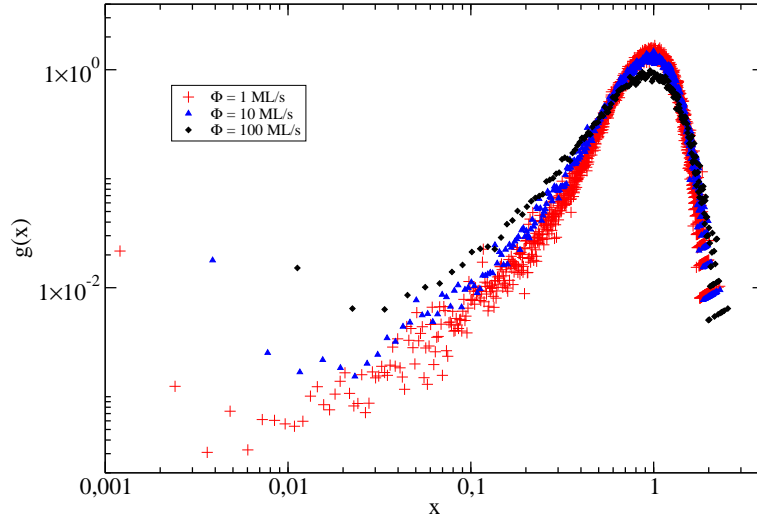


Figure 4. (Colour online) Scaled island size distribution for incident fluxes $\Phi = 1, 10$ and 100 ML/s from KMC simulations. In all cases, data have been taken at the saturation coverage of $\theta = 0.15$. See text for details.

a flux of 100 ML/s and at first keeping $T = 500$ K allows us to quantitatively compare the KRE results to those obtained from KMC in figures 3 and 4. The advantage of the KRE approach over KMC is evident in that the KRE data can be averaged over several hundreds of runs here with relatively modest computational effort. At this stage it is also interesting to compare the KRE predictions in two different growth modes. The KRE approach easily allows adjustment of the various average rates in the kinetic equation. To this end, we consider here two different growth modes. In the so-called limited adatom-island mode, only adatoms are mobile while the islands are immobile. This should be a reasonable approximation at low temperatures (as compared to E_d)

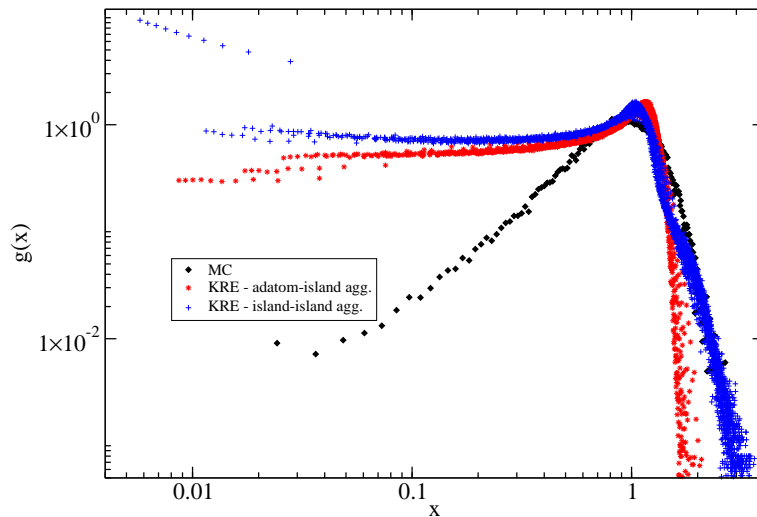


Figure 5. (Colour online) Comparison between KMC simulations and KRE data in the adatom-island and island-island growth modes at $T = 500$ K.

when the single adatom diffusion coefficient D_1 is much larger than that of the dimers. As seen in figure 2, this is not an unreasonable approximation at $T = 500$ K. In the second island-island mode, we solve the full KRE equations keeping all the diffusion coefficients presented in figure 2.

Comparison between the two different KRE growth modes and the KMC results are shown in figure 5. First, it can be observed that even at this temperature the adatom-island aggregation mode causes significant changes in the scaled distribution for larger island sizes, which are strongly influenced by zero island mobility. In contrast, the KMC and island-island mode KRE results are in excellent agreement for $x > 5$. There is, however, significant difference in $g(x)$ for small island sizes. This is in part due to the mean-field nature of the KRE theory, which underestimates fluctuation-induced nucleation of small islands, and in part due to the approximation of neglecting adatom detachment from islands, which also enhances aggregation of smaller islands to larger ones.

Finally, in figure 6 we show results from KRE for $T = 1000$ K. In this case, large fluctuations and finite-size effects prevented us from obtaining any statistically meaningful KMC data. It is interesting to note that while the adatom-island mode data shows very little temperature dependence as compared to the case where $T = 500$ K, the distribution for the island-island mode is qualitatively different from that of figure 5. There is a significant enhancement of small islands in the regime $x \ll 1$, which indicates that in this case neglecting the mobility of islands leads to significant errors in $g(x)$. This can be expected since figure 2 shows that at $T = 1000$ K island mobility is no longer orders of magnitude smaller than the single adatom mobility.

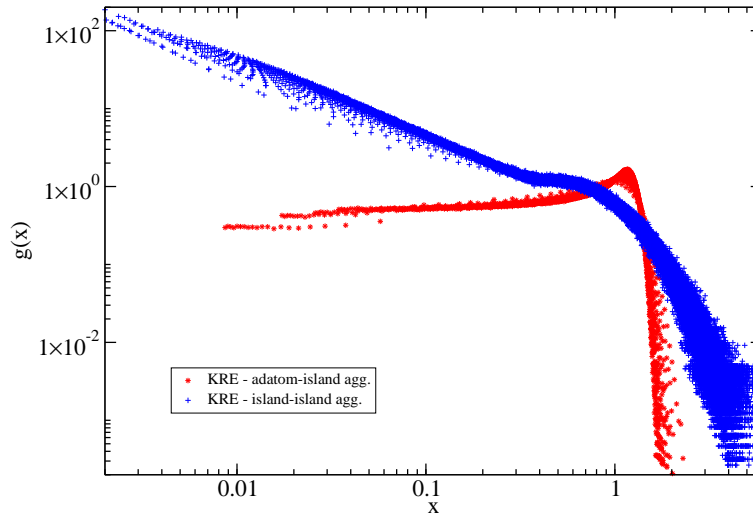


Figure 6. (Colour online) Results of KRE for the adatom-island and island-island modes at temperature $T = 1000$ K. In this case, it was not possible to obtain KMC data.

5. Conclusions

In this paper, we have presented a multi-scale study of growth of submonolayer 2D Fe islands on the Mo(110) surface. By using data from *ab initio* electronic structure calculations, we obtained the single-particle diffusion barrier E_d from the adiabatic potential surface seen by a single Fe adatom. The same calculations were used to determine interactions between pairs of Fe atoms up to 6th nearest neighbor pairs. These were used to construct a simple lattice-gas Hamiltonian in equation (1). Such a Hamiltonian is immediately amenable to direct KMC simulations of growth; however, to study time and especially length scales relevant to MBE growth a coarse-grained approach is beneficial. To this end we employed the KRE approach within the framework of a simple aggregation model of islands. The adatom island diffusion coefficients, which are needed as input to KRE, were determined from equilibrium MC simulations using the lattice-gas Hamiltonian, up to sizes of a few tens of atoms at $T = 500$ and 1000 K. These data were further used to simplify the interactions by including them up to 3rd nearest neighbors only in the Hamiltonian.

Following construction of the KMC and KRE models we then carried out actual MBE growth simulations for both models at the saturation coverage $\theta = 0.15$. Tests using the KMC data revealed that the scaled distribution function of island sizes $g(x)$ is rather insensitive to the flux in the regime between about 1 and 100 ML/s, and thus the latter value was used in most cases to facilitate comparison between KMC and KRE data. At $T = 500$ K such a comparison revealed that the mean-field type KRE model gives very good agreement in the full island-island mode with KMC data for large islands, but the agreement is poor for the smallest islands, where KRE overestimates the regime $x \ll 1$. Comparison between island-island and adatom-island modes in the

KRE model also reveals that at this temperature including single adatom mobility only gives reasonably good results for $g(x)$. On the other hand, the same comparison at $T = 1000$ K (where KMC simulations could not be performed even with 100 ML/s) shows that the scaled distribution function is even qualitatively wrong if island mobility is not included in the KRE aggregation rates.

Acknowledgments

The authors acknowledge the support from the Grant Agency of the Czech Republic under Contract No. 202/09/0775, and by joint funding under EU STRP 016447 MagDot and NSF DMR Award No. 0502737. This work has also been supported in part by the Academy of Finland through its COMP Centre of Excellence Program (project No. 251748). Computer resources provided by CSC-Center for Scientific Computing Ltd. are also acknowledged.

References

- [1] Venables J A, Spiller G D T and Hanbucken M 1984 *Reports on Progress in Physics* **47** 399
- [2] Reichelt K 1988 *Vacuum* **38** 1083 – 1099
- [3] Michely T and Krug J 2004 *Islands, mounds, and atoms: patterns and processes in crystal growth far from equilibrium* vol 42 (Springer Verlag)
- [4] Kotrla M 1996 *Computer Physics Communications* **97** 82–100
- [5] Jonsson H 2011 *Proceedings of the National Academy of Sciences* **108**(3) 944–949
- [6] Nandipati G, Shim Y and Amar J G 2010 *Phys. Rev. B* **81**(23) 235415
- [7] Stoldt C R, Jenks C J, Thiel P A, Cadilhe A M and Evans J W 1999 *Journal of Chemical Physics* **111** 5157–5166
- [8] Koponen I, Rusanen M and Heinonen J 1998 *Phys. Rev. E* **58** 4037–4040
- [9] Koponen I T, Jahma M O, Rusanen M and Ala-Nissila T 2004 *Phys. Rev. Lett.* **92** 086103
- [10] Evans J W, Thiel P and Bartelt M 2006 *Surface Science Reports* **61** 1
- [11] Hubartt B C, Kryukov Y A and Amar J G 2011 *Phys. Rev. E* **84** 021604
- [12] Köhler U, Jensen C, Schindler A, Brendel L and Wolf D 2000 *Philosophical Magazine Part B* **80** 283–292
- [13] Köhler U, Jensen C, Wolf C, Schindler A, Brendel L and Wolf D 2000 *Surf. Sci.* **454** 676–680
- [14] Fruchart O, Jubert P, Eleoui M, Cheynis F, Borca B, David P, Santonacci V, Liénard A, Hasegawa M and Meyer C 2007 *Journal of Physics: Condensed Matter* **19** 053001
- [15] Reshöft K, Jensen C and Köhler U 1999 *Surf. Sci.* **421** 320–336
- [16] Marchenko I 2007 *Vacuum* **81** 700–707
- [17] Yu Y M, Backofen R and Voigt A 2008 *Phys. Rev. E* **77**(5) 051605
- [18] Rogowska J 2002 *Surf. Sci.* **507** 340–345
- [19] Goykolov D and Kotrla M 2009 *Central European Journal of Physics* **7** 220–226
- [20] Boisvert G, Lewis L J and Scheffler M 1998 *Phys. Rev. B* **57** 1881–1889
- [21] Gollisch H 1986 *Surf. Sci.* **175** 249–262
- [22] Malzbender J, Przybylski M, Giergiel J and Kirschner J 1998 *Surf. Sci.* **414** 187 – 196
- [23] Jubert P O, Fruchart O and Meyer C 2001 *Phys. Rev. B* **64** 115419
- [24] Brune H, Bromann K, Röder H, Kern K, Jacobsen J, Stoltze P, Jacobsen K and Nørskov J 1995 *Physical Review B Condensed Matter* **52** 14380–14383
- [25] Schroeder M and Wolf D E 1997 *Surface science* **375** 129–140

- [26] Sabiryanov R, Cho K, Larsson M, Nix W and Clemens B 2003 *Journal of magnetism and magnetic materials* **258** 365–368
- [27] Clarke S and Vvedensky D 1988 *Journal of Applied Physics* **63** 2272–2283
- [28] Ratsch C, Zangwill A, Šmilauer P and Vvedensky D D 1994 *Phys. Rev. Lett.* **72** 3194–3197
- [29] Murphy S, MacMathuna D, Mariotto G and Shvets I V 2002 *Phys. Rev. B* **66**(19) 195417
- [30] Vanderbilt D 1990 *Phys. Rev. B* **41**(11) 7892–7895
- [31] Kresse G and Furthmüller J 1996 *Phys. Rev. B* **54**(16) 11169–11186
- [32] Kresse G and Furthmüller J 1996 *Comput. Mater. Sci.* **54**(6) 15
- [33] Perdew J P, Chevary J A, Vosko S H, Jackson K A, Pederson M R, Singh D J and Fiolhais C 1992 *Phys. Rev. B* **46**(11) 6671–6687
- [34] Ala-Nissila T, Kjoll J and Ying S C 1992 *Phys. Rev. B* **46** 846–854
- [35] Vattulainen I, Merikoski J, Ala-Nissila T and Ying S C 1998 *Phys. Rev. B* **57** 1896
- [36] Ala-Nissila T, Ferrando R and Ying S C 2002 *Adv. Phys.* **51**(3) 949
- [37] Ying S C, Vattulainen I, Merikoski J, Hjelt T and Ala-Nissila T 1998 *Phys. Rev. B* **58** 2170
- [38] S C Wang and G Ehrlich 1990 *Surf. Sci.* **239** 301
- [39] S C Wang and U Kürpick and G Ehrlich 1998 *Phys. Rev. Lett.* **81** 4923
- [40] Kyuno K and Ehrlich G 2000 *Phys. Rev. Lett.* **84** 2658
- [41] Heinonen J, Koponen I T, Merikoski J and Ala-Nissila T 1999 *Phys. Rev. Lett.* **82** 2733
- [42] Trushin O S, Salo P and Ala-Nissila T 2000 *Phys. Rev. B* **62** 1611
- [43] Salo P, Hirvonen J, Koponen I S, Trushin O S, Heinonen J and Ala-Nissila T 2001 *Phys. Rev. B* **64** 161405
- [44] Trushin O S, Salo P, Alatalo M and Ala-Nissila T 2001 *Surf. Sci.* **482-485** 365
- [45] Heinonen J, Salo P, Alatalo M, Ala-Nissila T, Koponen I T and Merikoski J 2001 *Collective Diffusion on Surfaces: Correlation Effects and Adatom Interactions*, ed. by M. C. Tringides and Z. Chvoj (Kluwer) pp 317–325
- [46] Khare S V, Bartelt N C and Einstein T L 1995 *Phys. Rev. Lett.* **75** 2148
- [47] Khare S V and Einstein T L 1996 *Phys. Rev. B* **54** 11752
- [48] Bartelt M C and Evans J W 1992 *Phys. Rev. B* **46** 12675
- [49] Bales G S and Chrzan D C 1994 *Phys. Rev. B* **50** 6057
- [50] Bales G S and Chrzan D C 1995 *Phys. Rev. Lett.* **74** 4879
- [51] Jahma M O, Rusanen M, Karim A, Koponen I T, Ala-Nissila T and Rahman T S 2005 *Surf. Sci.* **598** 246
- [52] Koponen I T, Jahma M O, Rusanen M and Ala-Nissila T 2004 *Phys. Rev. Lett.* **92** 086103–1
- [53] Maksym P A 1988 *Semicond. Sci. Technol.* **3** 594–596
- [54] Shim Y and Amar J G 2012 *Phys. Rev. Lett.* **108**(7) 076102
- [55] Kang K and Redner S 1984 *Phys. Rev. Lett.* **52** 955
- [56] Krapivsky P L, Mendes J F F and Redner S 1998 *Eur. Phys. J. B* **4** 401–404